Observation of magnetically-induced transition intensity redistribution in the onset of the hyperfine Paschen-Back regime

Armen Sargsyan^a, Emmanuel Klinger^{b,*}, Ara Tonoyan^a, David Sarkisyan^a

^aInstitute for Physical Research – National Academy of Sciences of Armenia, 0203 Ashtarak-2, Armenia

Abstract

The Zeeman effect is an important topic in atomic spectroscopy. The induced change in transition frequencies and amplitudes finds applications in the Earth-field-range magnetometry. At intermediate magnetic field amplitude $B \sim B_0 = A_{\rm hfs}/\mu_B$, where $A_{\rm hfs}$ is the magnetic dipole constant of the ground state, and μ_B is the Bohr magneton ($B_0 \approx 1.7 \,\mathrm{kG}$ for Cs), the rigorous rule $\Delta F = 0, \pm 1$ is affected by the coupling between magnetic sublevels induced by the field. Transitions satisfying $\Delta F = \pm 2$, referred to as magnetically-induced transitions, can be observed. Here, we show that a significant redistribution of the Cs $6S_{1/2} \rightarrow 6P_{3/2}$ magnetically-induced transition intensities occurs with increasing magnetic field. We observe that the strongest transition in the group $F_g = 3 \rightarrow F_e = 5 \ (\sigma^+ \text{ polarization})$ for $B < B_0$ cease to be the strongest for $B > 3 B_0$. On the other hand, the strongest transition in the group $F_g = 2 \rightarrow F_e = 4$ (σ^- polarization) remains so for all our measurements with magnetic fields up to 9 kG. These results are in agreement with a theoretical model. The model predicts that similar observations can be made for all alkali metals, including Na, K and Rb atoms. Our findings are important for magnetometers utilizing the Zeeman effect above Earth field, following the rapid development of micro-machined vapor-cell-based sensors.

Keywords: Sub-Doppler spectroscopy, nanocell, Cs D₂ line, magnetic field

^b Université de Franche-Comté, SupMicroTech-ENSMM, UMR 6174 CNRS, Institut FEMTO-ST, 25030 Besançon, France

^{*}emmanuel.klinger@femto-st.fr

1. Introduction

Hot atomic vapors of alkali metal atoms are at the core of many fundamental and applied precision physics experiments. They can be used in the search for signatures of beyond-the-Standard-Model physics [1], and possess a large range of applications. In contrast to other technologies with similar performances, vapor-cell-based sensors have been receiving a lot of attention because of the possibilities for miniaturization and low power consumption while retaining their sensitivities [2].

The Zeeman effect occurs when atoms are in the presence of an external magnetic field. Hyperfine levels are split, and transition frequencies and intensities undergo significant changes as a function of the field magnitude [3, 4]. At intermediate magnetic field amplitude $B \sim B_0 = A_{\rm hfs}/\mu_B$, where $A_{\rm hfs}$ is the magnetic dipole constant of the ground state, and μ_B is the Bohr magneton ($B_0 \approx 1.7\,{\rm kG}$ for Cs), the coupling between magnetic sub-levels induced by the field leads to an ambiguous set of transition selection rules. Transitions satisfying $\Delta F = \pm 2$, referred to as magnetically-induced transitions (MI), can be observed while being forbidden at zero field. As demonstrated in previous studies [5, 6], the intensity of MI transitions satisfying the condition $F_e - F_g \equiv \Delta F = +2$ is the greatest with σ^+ polarized radiation, while MI transitions satisfying the condition $\Delta F = -2$ exhibit the greatest intensity with σ^- polarized radiation.

At low and intermediate field, these transitions are often overlooked, as conventional weak-probe spectroscopy is not enough to properly resolve individual transitions because of the Doppler effect [7]. On the other hand, sub-Doppler spectra obtained with non-linear techniques can be difficult to interpret. With nanocells (NCs), however, one can directly obtain sub-Doppler spectra while remaining in the weak-probe regime of interaction. In these cells, the vapor is confined between two almost-parallel windows with a separation spanning from a few nm to a few μ m. The confinement of the vapor to dimensions on the order of the probe optical wavelength leads to the (optical) Dicke-type coherent narrowing [8], well known in the microwave domain [9]. In addition to spectroscopy, NC are an important tool in fundamental physics: they can for example be used to study atom-surface interactions [10, 11], cooperative effects [12, 13], and single photon generation [14].

Magnetically-induced transitions can be utilized as novel frequency mark-

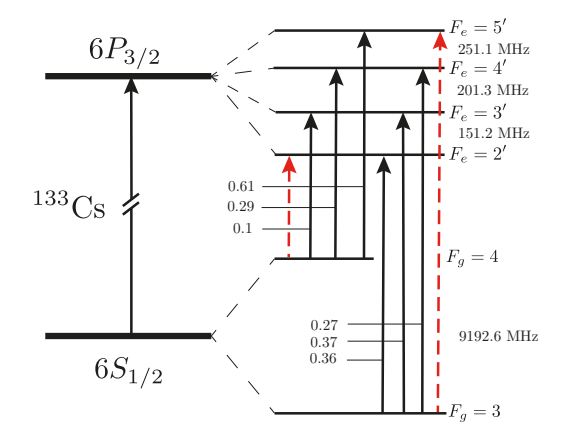


Figure 1: Hyperfine transition diagram of the Cs atom D_2 line indicating splittings between hyperfine levels and relative transition strength factors. The dashed red arrows indicate the transitions that are forbidden at zero magnetic field (MI transitions), subject of this study.

ers in high magnetic fields, enabling the exploration of new frequency ranges and facilitating the frequency stabilization of lasers operating at significantly shifted frequencies compared to the initial transitions in unperturbed atoms [15]. Magnetically-induced transitions in Cs and Rb have also found successful applications in the process of electromagnetically induced transparency in strong magnetic fields [16–18]. The complete understanding of the evolution of alkali transitions in a magnetic field is important for high field magnetometry [19–23]. As these magnetometers are based on optical readout, they are compatible with harsh environments applications [24]. Consequently, it is important to investigate the behavior of MI transitions in magnetic fields exceeding B_0 .

In this article, we study the absorption spectrum of Cs atoms confined in a NC, and placed in a magnetic field spanning over a few kG. We show that the strongest transition in the group $F = 3 \rightarrow 5'$ (σ^+ polarization) of the D₂ line, see Fig. 1, for $B < B_0$ cease to be the strongest for $B > 3 B_0$. On the other hand, the strongest transition in the group $F = 2 \rightarrow 4'$ (σ^- polarization) remains so for all magnetic field values, in agreement with a theoretical modeling of thin vapor layer absorption spectrum of alkali atoms placed in a magnetic field, see Sec. 2. The experimental setup and results are presented in Sec. 3.

2. Spectrum of Cs atoms in a magnetic field

2.1. Absorption profile

The absorption profile of atoms confined in nanocells is fundamentally different from that of a usual vapor cell. In the case of a nanocell, the atomic response is dominated by a large spatial dispersion [25]. The profile strongly depends on the thickness ℓ of the probed vapor layer [8]. In the weak-probe regime, one can model the system as an ensemble of two-level systems interacting with light of angular frequency ω_l and wavevector k, see e.g. Ref. [6]. Each two-level system has a transition frequency and a dipole moment that depend on the magnitude of the magnetic field. The transmission spectrum is then obtained by summing over all possible transitions j:

$$S_t \propto \frac{1}{|Q|^2} \cdot \sum_j \operatorname{Im} \left[\chi_j(\omega_l, \ell, B) \right],$$
 (1)

where $Q = 1 - r^2 \exp(2ik\ell)$ and r is the (field) reflection coefficient of the cell windows. An analytical expression for the transition lineshape of a two-level system was derived in Ref. [26], it reads

$$\chi_j(\omega_l, \ell, B) = -4(1 - r \exp[ik\ell])^2 \cdot \frac{\sin(k\ell/2)}{Q} \cdot \frac{\mathcal{N}}{ku\sqrt{\pi}} \cdot \frac{iA_j}{\Gamma/2 - i\Delta_j}, \tag{2}$$

where \mathcal{N} is the vapor density, $u(\Theta) = \sqrt{2k_B\Theta/m_a}$ is the thermal velocity at a temperature Θ for atoms of mass m_a . The (magnetic-field dependent) transition parameters $\Delta_j = \omega_l - \omega_j$ and A_j (proportional to the squared dipole moment) are derived in the next section. The homogenous broadening Γ , including contributions from natural linewidth, collisional broadening, etc., is left as a free parameter in our simulations.

2.2. Zeeman effect

The theoretical description of the Zeeman effect on the spectrum of alkali atoms is extensively detailed in various studies [3, 4, 27–30]. In the presence of magnetic field, the magnetic sublevels are split leading to changes in transition probabilities and frequencies. This can be calculated by diagonalizing the Hamiltonian matrix accounting for the hyperfine atomic structure, and the interaction with the magnetic field

$$H = H_{\rm hfs} + \frac{\mu_B}{\hbar} (g_S S_z + g_L L_z + g_I I_z) B_z , \qquad (3)$$

where $g_{S,L,I}$ are the Landé factors [31, 32] and S_z , L_z , I_z the projection of quantum numbers on the z-axis (quantization axis). The eigenvalues give the energy levels, needed to calculate the transition frequencies, and the eigenvectors are used to calculate the transition dipole moments

$$|\langle e||d||g\rangle|^2 \propto \Gamma_{\rm N} a^2 [\psi(F'_e, m_{F_e}); \psi(F'_q, m_{F_g}); q],$$
 (4)

with Γ_N the natural linewidth of the transition. The transfer coefficients are calculated with

$$a[\psi(F'_e, m_{F_e}); \psi(F'_g, m_{F_g}); q] = \sum_{F_e, F_g} C_{F'_e, F_e} a(F'_e, m_{F_e}; F'_g, m_{F_g}; q) C_{F'_g, F_g}, \quad (5)$$

where $C_{F'F}$ are the mixing coefficients (obtained from the eigenvectors). The coefficient $a(F'_e, m_{F_e}; F'_g, m_{F_g}; q)$ reads

$$a(F'_{e}, m_{F_{e}}; F'_{g}, m_{F_{g}}; q) = (-1)^{1+I+J_{e}+F_{e}+F_{g}-m_{F_{e}}} \sqrt{2J_{e}+1} \sqrt{2F_{e}+1} \times \sqrt{2F_{g}+1} \begin{pmatrix} F_{e} & 1 & F_{g} \\ -m_{F_{e}} & q & m_{F_{g}} \end{pmatrix} \begin{Bmatrix} F_{e} & 1 & F_{g} \\ J_{g} & I & J_{e} \end{Bmatrix},$$
 (6)

where $q=0,\pm 1$ is associated with the polarization of the incident laser field. In the previous equation, the parentheses (curly brackets) denotes 3-j (6-j) coefficients.

The calculated MI transition intensities are shown in Fig. 2. A striking example of a gigantic increase in transition intensity is the behavior of the $F=3\to 5'$ transitions (seven transitions) and $F=2\to 4'$ (five transitions) of the Cs D_2 line. Note that the excited state quantum numbers are denoted with primes. In the range of $0.5-1\,\mathrm{kG}$, the intensities of these transitions increase greatly, especially for σ^+ circularly polarized radiation. Three of them (⑤,⑥, and ⑦) have the highest probabilities in the range of $0.5-2\,\mathrm{kG}$ among all transitions originating from $F_g=3$ [28]. Magnetically-induced transitions have interesting characteristics: (i) they remain observable with magnetic fields as high as $B_z\sim 8\,\mathrm{kG}$; (ii) they are located either in the high-frequency wing of the spectrum (for $F=3\to 5'$) or in the low-frequency wing of the spectrum (for $F=4\to 2'$), see Fig. 3, without intersecting much with other Cs transitions; (iii) for $B_z\sim 8\,\mathrm{kG}$, the frequency shift of transitions reaches about $\pm 35\,\mathrm{GHz}$ in the case of σ^\pm polarization, with respect to the weighed center of the Cs D_2 line.

From Figure 2, we can see that transition 5^* remains the strongest one in the $4 \to 2'$ group, in the whole magnetic field range where it is measurable.

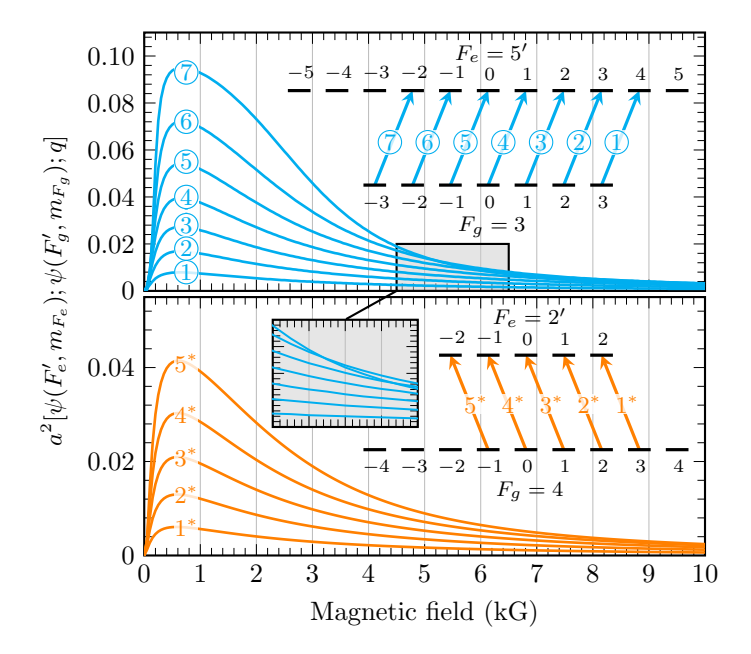


Figure 2: Calculated probabilities of $F_g=4\to 2'$ transitions $(q=-1,\ {\rm bottom})$ and $F_g=3\to 5'$ transitions $(q=1,\ {\rm top})$ plotted against magnetic field. The inset plot shows a zoom on magnetic fields ranging from 4.5 to 6.5 kG. Transition diagrams and labeling are shown as insets.

On the other hand, transition \bigcirc is the strongest one only up to about $3B_0 \approx 5.1 \,\mathrm{kG}$, see the inset in Fig 2. Above $5B_0$, two MI transitions emerge as the strongest in the group of $F = 3 \rightarrow 5'$: transitions \bigcirc and \bigcirc .

The magnetic field dependence of the frequency shift for the seven MI transitions $F=3 \rightarrow 5'$ and five transitions $F=4 \rightarrow 2'$ is depicted in Figure 3. Beyond $B_z=3.5\,\mathrm{kG}$, both groups of transitions become distinctly separated, which holds significance for applications involving MI transitions, for example for laser frequency stabilization [15].

3. Experiment

The experimental setup is depicted in Figure 4. A tunable external-cavity diode laser (ECDL) emitting at a wavelength $\lambda = 852\,\mathrm{nm}$ with a spectral linewidth of less than 1 MHz is tuned in the vicinity of the Cs D₂ line. Single-beam sub-Doppler spectroscopy is achieved by illuminating the nanocell with a 1 mm-diameter laser beam in the region having a thickness $\ell = \lambda/2 \approx 426\,\mathrm{nm}$ [8, 33]. This region is indicated in the inset of Figure 4. Details on

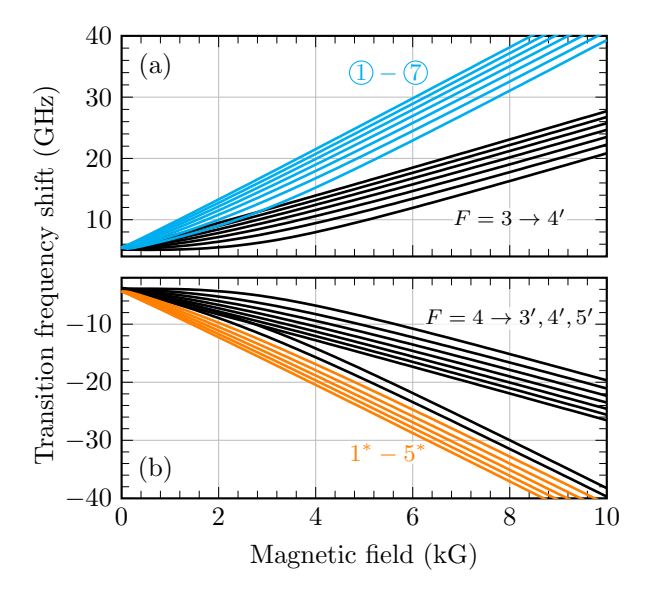


Figure 3: Transition frequency shift as a function of the magnetic field. (a) $F = 3 \rightarrow 4', 5'$ transitions in the case of σ^+ -polarized light, including the \bigcirc – \bigcirc MI transitions (cyan). (b) $F = 4 \rightarrow 2', 3', 4', 5'$ transitions in the case of σ^- -polarized light, including the $1^* - 5^*$ MI transitions (orange). The frequency shifts are calculated with respected to the weighed center of the Cs D₂ line.

the nanocell fabrication process and its oven can be found in Ref. [34]. In addition to increasing the spectral resolution, using a NC also allows to record the spectrum in the linear regime of interaction between light and atoms. This is convenient to directly compare the amplitude of the absorption peaks and extract ratios of amplitudes. The cell temperature is set to 100° C, and the power of the laser beam was about $15 \,\mu\text{W}$. At this temperature, the Cs vapor pressure is 6.1×10^{-4} Torr and the number density is 1.6×10^{13} cm⁻³.

Magnetic fields ranging from $B_z = 1 \,\mathrm{mT}$ to 0.9 T are applied using a robust permanent ring magnets system mounted on a translation stage [35]. Despite a large gradient (with respect to e.g. a pair Helmholtz coils), the spectral resolution is acceptable when using permanent magnets: transitions are additionally broadened by only a few tens of MHz. This is because of the small thickness of probed layer [36]. Note that the field inhomogeneities could be reduced using the "magic sphere" configuration [37], as was shown in Ref. [38]. The magnetic field is aligned with the propagation direction of the laser radiation, so that σ^{\pm} transition can be observed. The light polarization is adjusted using a quarter-wave plate placed before the NC-oven assembly.

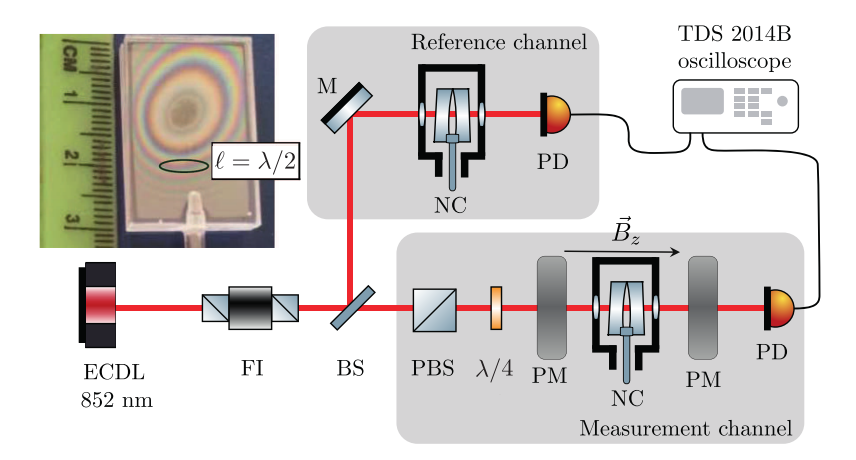


Figure 4: Sketch of the experimental setup. ECDL – extended cavity diode laser, FI – Faraday isolator, BS – beam splitter, M – mirror, PBS – polarizing beam splitter, NC – Cs nanocell in the oven, $\lambda/4$ – quarter-wave plate, PM – permanent ring magnets, PD – photodetectors. The inset shows a picture of the Cs nanocell where the thickness $\ell=\lambda/2\approx 426\,\mathrm{nm}$ is indicated.

Approximately 30% of the laser radiation is split off to form a frequency reference channel [6]. The change of light intensity by propagating through the nanolayer of alkali is captured with photodiodes whose signal is fed to a four-channel oscilloscope (Tektronix TDS2014B).

Figure 5 shows examples of absorption spectra recorded from the nanocell at various magnitude of the magnetic field for σ^+ (top) and σ^- (bottom) laser polarization. In these spectra, all 12 MI transitions (① to ⑦ and 1* to 5*) for both circular polarizations are observed and well resolved. Fits of the model described in Sec. 2 to experimental data (black dots) are shown with red solid lines. A good agreement between experiment and theory can be seen. For $B_z < 3B_0$ [Fig. 5(a)], the transition $|3, -3\rangle \rightarrow |5', -2'\rangle$, labeled ⑦, is seen to be larger than $|3, -2\rangle \rightarrow |5', -1'\rangle$, labeled ⑥. Note that states are expressed in the coupled basis of states $|F, m_F\rangle$; for the complete set of labels, see the inset in Fig. 2. However, when $B_z > 3B_0$ [Fig. 5(b)], transition ⑥ is seen to be the largest one among the seven σ^+ MI transitions of this group. In contrast, the transition $|4, -1\rangle \rightarrow |2', -2'\rangle$, labeled 5* remains the strongest one, [see Fig. 5(c) and (d)].

The magnetic-field dependence of the ratio between the strongest MI transitions in the case of σ^{+-} (cyan) and σ^{--} (orange) polarized light is shown

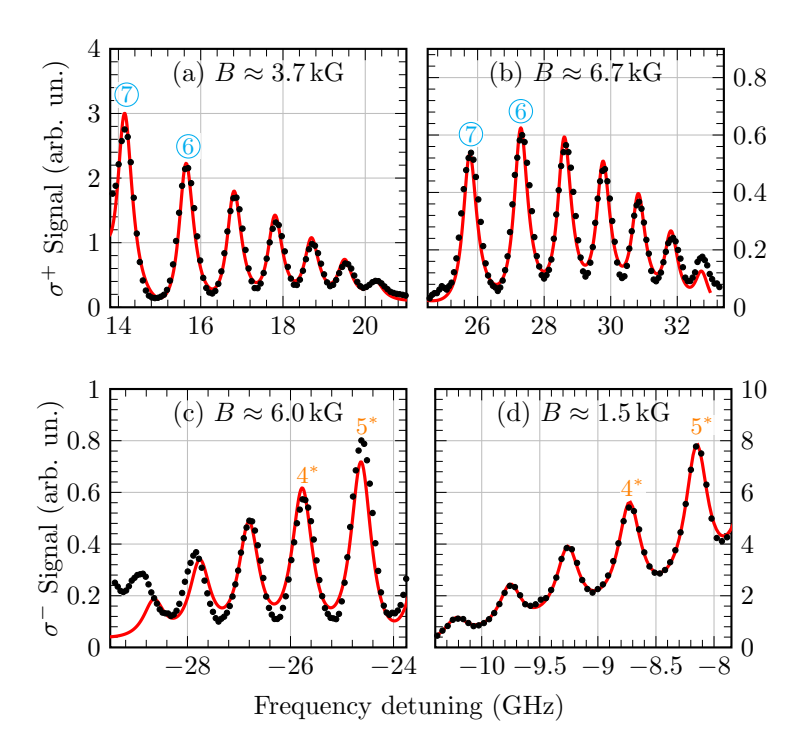


Figure 5: Examples of Cs D_2 line absorption spectrum in a magnetic field for (a-b) σ^+ -polarized light, (c-d) σ^- -polarized light recorded with 32 averages. The model discussed in Sec. 2 (red lines) was fit to the experimental data (black dots). Depending on the magnitude of the magnetic field, fitted linewidths ranging from 50-75 MHz were extracted from the fits. The zero frequency detuning corresponds to the frequency of the that of the $6S_{1/2} \rightarrow 6P_{3/2}$ transition.

in Fig. 6. The experimental data (dots) were obtained by simply dividing the on-resonance signal of the transitions. The amplitude of the error bars corresponds to the measured voltage noise on the peaks of interest. Below $3B_0 \approx 5.1 \,\mathrm{kG}$, transitions 7 and 5 have the largest amplitude. However, one can observe that, above $3B_0$, transition 6 becomes larger than 7 (ratio below 1). Transition 5 remains stronger than 4 in the whole range of measurements. Despite the simple method used to extract the peak amplitude, these observations align with the calculated ratios of MI transition intensities as a function of magnetic field (solid lines in Fig. 6). This can be useful, for example for large field magnetometers utilizing quick algorithms to find the peak heights and positions and deduce the magnetic field seen by the atoms.

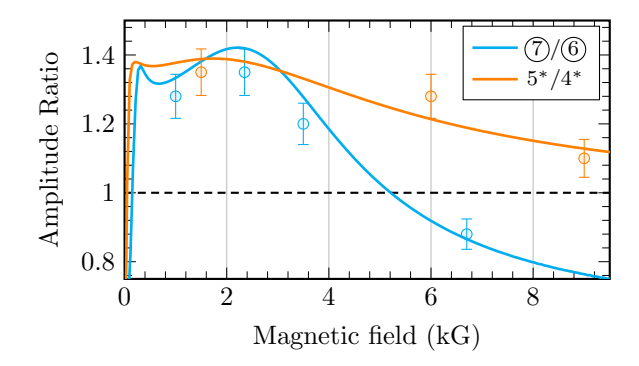


Figure 6: Evolution of transition amplitude ratio as a function of applied magnetic field for the two strongest σ^+ (cyan dots) and σ^- (orange dots) MI transitions. The amplitude of the error bars corresponds to the measured voltage noise on the peaks of interest. The lines show the theoretical ratio. The case where the amplitude of both transitions are equal is indicated with a dashed line.

4. Conclusion

We have studied the behavior of magnetically-induced transitions in magnetic fields up to 9 kG by means of linear transmission spectroscopy from a nanocell. A large redistribution of the intensities with increasing magnetic field is observed. In particular, the σ^+ MI transition $|3, -3\rangle \rightarrow |5', -2'\rangle$ cease to be the most intense at field above $3 B_0$. In contrast, the σ^- MI transition $|4, -1\rangle \rightarrow |2', -2'\rangle$ is observed to remain the strongest in the whole range of investigated magnetic field. A simple reading of the on-resonance signal is found to yield results in agreement with a theoretical modeling of thin vapor layer absorption spectrum of alkali atoms placed in a magnetic field. The model predicts a similar behavior for MI transitions of other alkali metals, including Na, K and Rb atoms. For example, the ⁸⁵Rb $|2, -2\rangle \rightarrow |4', -1'\rangle$ MI transition cease to be the strongest one in the group $F = 2 \rightarrow 4'$ above $3B_0(^{85}\text{Rb}) \sim 2.1 \,\text{kG}$ while the MI transition $|3,0\rangle \rightarrow |1', -1'\rangle$ remains the strongest one in the group $F = 3 \rightarrow 1'$.

These results could be beneficial to large field magnetometers utilizing the Zeeman effect. With quick algorithms to find the peak heights and positions to deduce the magnetic field seen by the atoms, one could improve the bandwidth of high-dynamic range magnetometers based on alkali D line spectrum fitting [22]. Because of a smaller sensitivity to field gradient, one could achieve better sensitivities in high pulsed field measurements [19] by using nanocells. To conclude, we note that our findings could also be use-

ful to enlarge the tuning range of group velocity manipulation for slow-light experiments using electromagnetically-induced transparency [39].

Acknowledgement

The authors would like to thank A. Amiryan for fruitful discussions. The work was supported by the Science Committee of RA, in the frame of the research project No 21T-1C005.

References

- [1] M. S. Safronova, D. Budker, D. DeMille, D. F. J. Kimball, A. Derevianko, C. W. Clark, Search for new physics with atoms and molecules, Rev. Mod. Phys. 90 (2018) 025008. doi:10.1103/RevModPhys.90.025008.
 - URL https://link.aps.org/doi/10.1103/RevModPhys.90.025008
- [2] J. Kitching, Chip-scale atomic devices, Applied Physics Reviews 5 (3) (2018) 031302. doi:https://doi.org/10.1063/1.5026238.
- [3] P. Tremblay, A. Michaud, M. Levesque, S. Thériault, M. Breton, J. Beaubien, N. Cyr, Absorption profiles of alkali-metal D lines in the presence of a static magnetic field, Phys. Rev. A 42 (5) (1990) 2766. doi:https://doi.org/10.1103/PhysRevA.42.2766.
- [4] M. Auzinsh, D. Budker, S. Rochester, Optically polarized atoms: understanding light-atom interactions, Oxford University Press, 2010.
- [5] A. Tonoyan, A. Sargsyan, E. Klinger, G. Hakhumyan, C. Leroy, M. Auzinsh, A. Papoyan, D. Sarkisyan, Circular dichroism of magnetically induced transitions for D₂ lines of alkali atoms, Eur. Phys. Lett. 121 (5) (2018) 53001. doi:https://doi.org/10.1209/0295-5075/ 121/53001.
- [6] A. Sargsyan, A. Amiryan, A. Tonoyan, E. Klinger, D. Sarkisyan, Circular dichroism in atomic vapors: magnetically induced transitions responsible for two distinct behaviors, Physics Letters A 390 (2021) 127114. doi:https://doi.org/10.1016/j.physleta.2020.127114.

- [7] D. Pizzey, J. D. Briscoe, F. D. Logue, F. S. Ponciano-Ojeda, S. A. Wrathmall, I. G. Hughes, Laser spectroscopy of hot atomic vapours: from 'scope to theoretical fit, New Journal of Physics 24 (12) (2022) 125001. doi:10.1088/1367-2630/ac9cfe.
- [8] G. Dutier, A. Yarovitski, S. Saltiel, A. Papoyan, D. Sarkisyan, D. Bloch, M. Ducloy, Collapse and revival of a dicke-type coherent narrowing in a sub-micron thick vapor cell transmission spectroscopy, Europhysics Letters 63 (1) (2003) 35.
- [9] R. H. Romer, R. H. Dicke, New technique for high-resolution microwave spectroscopy, Phys. Rev. 99 (2) (1955) 532.
- [10] A. Laliotis, B.-S. Lu, M. Ducloy, D. Wilkowski, Atom-surface physics: A review, AVS Quantum Science 3 (4) (2021) 043501. arXiv:https: //doi.org/10.1116/5.0063701, doi:10.1116/5.0063701. URL https://doi.org/10.1116/5.0063701
- [11] A. Sargsyan, R. Momier, C. Leroy, D. Sarkisyan, Competing van der waals and dipole-dipole interactions in optical nanocells at thicknesses below 100 nm, Physics Letters A 483 (2023) 129069. doi:https://doi.org/10.1016/j.physleta.2023.129069. URL https://www.sciencedirect.com/science/article/pii/ S0375960123004498
- [12] J. Keaveney, A. Sargsyan, U. Krohn, I. G. Hughes, D. Sarkisyan, C. S. Adams, Cooperative Lamb Shift in an Atomic Vapor Layer of Nanometer Thickness, Phys. Rev. Lett. 108 (2012) 173601. doi:10.1103/PhysRevLett.108.173601. URL https://link.aps.org/doi/10.1103/PhysRevLett.108. 173601
- [13] T. Peyrot, Y. R. P. Sortais, J.-J. Greffet, A. Browaeys, A. Sargsyan, J. Keaveney, I. G. Hughes, C. S. Adams, Optical Transmission of an Atomic Vapor in the Mesoscopic Regime, Phys. Rev. Lett. 122 (2019) 113401. doi:10.1103/PhysRevLett.122.113401. URL https://link.aps.org/doi/10.1103/PhysRevLett.122.113401

- [14] F. Ripka, H. Kübler, R. Löw, T. Pfau, A room-temperature singlephoton source based on strongly interacting Rydberg atoms, Science 362 (6413) (2018) 446–449.
- [15] A. Sargsyan, A. Tonoyan, R. Mirzoyan, D. Sarkisyan, A. M. Wojciechowski, A. Stabrawa, W. Gawlik, Saturated-absorption spectroscopy revisited: atomic transitions in strong magnetic fields (< 20 mT) with a micrometer-thin cell, Opt. Lett. 39 (8) (2014) 2270–2273. doi: 10.1364/0L.39.002270.</p>
- [16] A. Sargsyan, A. Tonoyan, A. Papoyan, D. Sarkisyan, Dark resonance formation with magnetically induced transitions: extension of spectral range and giant circular dichroism, Optics letters 44 (6) (2019) 1391– 1394.
- [17] A. Sargsyan, A. Tonoyan, R. Momier, C. Leroy, D. Sarkisyan, Formation of strongly shifted eit resonances using "forbidden" transitions of cesium, Journal of Quantitative Spectroscopy and Radiative Transfer 303 (2023) 108582.
- [18] A. Sargsyan, A. Tonoyan, D. Sarkisyan, Application of magnetically induced $F_g = 4 \rightarrow F_e = 2$ atomic transitions of cesium atoms in strong magnetic fields, Optics Communications 537 (2023) 129464.
- [19] S. George, N. Bruyant, J. Béard, S. Scotto, E. Arimondo, R. Battesti, D. Ciampini, C. Rizzo, Pulsed high magnetic field measurement with a rubidium vapor sensor, Review of Scientific Instruments 88 (7) (2017) 073102. arXiv:https://pubs.aip.org/aip/rsi/article-pdf/doi/10.1063/1.4993760/14786267/073102_1_online.pdf, doi:10.1063/1.4993760. URL https://doi.org/10.1063/1.4993760
- [20] D. Ciampini, R. Battesti, C. Rizzo, E. Arimondo, Optical spectroscopy of a microsized rb vapor sample in magnetic fields up to 58 t, Physical Review A 96 (5) (2017) 052504.
- [21] J. Keaveney, F. S. Ponciano-Ojeda, S. M. Rieche, M. J. Raine, D. P. Hampshire, I. G. Hughes, Quantitative optical spectroscopy of 87rb vapour in the voigt geometry in dc magnetic fields up to 0.4 t, Journal of Physics B: Atomic, Molecular and Optical Physics 52 (5) (2019) 055003.

- [22] E. Klinger, H. Azizbekyan, A. Sargsyan, C. Leroy, D. Sarkisyan, A. Papoyan, Proof of the feasibility of a nanocell-based wide-range optical magnetometer, Appl. Opt. 59 (8) (2020) 2231–2237. doi:10.1364/AO. 373949.
- [23] H. Stærkind, K. Jensen, J. H. Müller, V. O. Boer, E. S. Polzik, E. T. Petersen, High-field optical cesium magnetometer for magnetic resonance imaging, arXiv preprint arXiv:2309.12006.
- [24] K.-M. C. Fu, G. Z. Iwata, A. Wickenbrock, D. Budker, Sensitive magnetometry in challenging environments, AVS Quantum Science 2 (4) (2020) 044702. arXiv:https://pubs.aip.org/avs/aqs/article-pdf/doi/10.1116/5.0025186/13816846/044702_1_online.pdf, doi:10.1116/5.0025186. URL https://doi.org/10.1116/5.0025186
- [25] A. V. Ermolaev, T. A. Vartanyan, Theory of thin-vapor-layer linear-optical properties: The case of quenching of atomic polarization upon collisions of atoms with dielectric walls, Phys. Rev. A 105 (2022) 013518. doi:10.1103/PhysRevA.105.013518. URL https://link.aps.org/doi/10.1103/PhysRevA.105.013518
- [26] G. Dutier, S. Saltiel, D. Bloch, M. Ducloy, Revisiting optical spectroscopy in a thin vapor cell: mixing of reflection and transmission as a fabry–perot microcavity effect, J. Opt. Soc. Am. B 20 (5) (2003) 793–800. doi:10.1364/JOSAB.20.000793.
- [27] E. B. Alexandrov, M. P. Chaika, G. I. Khvostenko, Interference of atomic states, Vol. 7, Springer, 1993.
- [28] A. Sargsyan, A. Tonoyan, G. Hakhumyan, A. Papoyan, E. Mariotti, D. Sarkisyan, Giant modification of atomic transition probabilities induced by a magnetic field: forbidden transitions become predominant, Laser Phys. Lett. 11 (5) (2014) 055701. doi:doi:10.1088/1612-2011/ 11/5/055701.
- [29] S. Scotto, D. Ciampini, C. Rizzo, E. Arimondo, Four-level N-scheme crossover resonances in Rb saturation spectroscopy in magnetic fields, Phys. Rev. A 92 (2015) 063810. doi:10.1103/PhysRevA.92.063810.

- [30] A. Sargsyan, E. Klinger, G. Hakhumyan, A. Tonoyan, A. Papoyan, C. Leroy, D. Sarkisyan, Decoupling of hyperfine structure of Cs D₁ line in strong magnetic field studied by selective reflection from a nanocell, J. Opt. Soc. Am. B 34 (4) (2017) 776–784.
- [31] B. Olsen, B. Patton, Y.-Y. Jau, W. Happer, Optical pumping and spectroscopy of Cs vapor at high magnetic field, Physical Review A 84 (6) (2011) 063410.
- [32] H. Stærkind, K. Jensen, J. H. Müller, V. O. Boer, E. T. Petersen, E. S. Polzik, Precision measurement of the excited state landé g-factor and diamagnetic shift of the cesium d 2 line, Physical Review X 13 (2) (2023) 021036.
- [33] A. Sargsyan, A. Amiryan, Y. Pashayan-Leroy, C. Leroy, A. Papoyan, D. Sarkisyan, Approach to quantitative spectroscopy of atomic vapor in optical nanocells, Opt. Lett. 44 (22) (2019) 5533–5536. doi:10.1364/OL.44.005533.
- [34] G. G. Gurzadyan, G. Y. Kryuchkyan, A. V. Papoyan, Modern optics and photonics: Atoms and structured media, World Scientific, p. 257, 2010.
- [35] A. Sargsyan, B. Glushko, D. Sarkisyan, Micron-thick spectroscopic cells for studying the paschen-back regime on the hyperfine structure of cesium atoms, J. Exp. and Theor. Phys. 120 (4) (2015) 579–586. doi:10.1134/S1063776115040159.
- [36] A. Sargsyan, G. Hakhumyan, A. Papoyan, D. Sarkisyan, A. Atvars, M. Auzinsh, A novel approach to quantitative spectroscopy of atoms in a magnetic field and applications based on an atomic vapor cell with L = λ, Applied Physics Letters 93 (2) (2008) 021119. doi:https://doi.org/10.1063/1.2960346.
- [37] G. Trénec, W. Volondat, O. Cugat, J. Vigué, Permanent magnets for faraday rotators inspired by the design of the magic sphere, Appl. Opt. 50 (24) (2011) 4788–4797. doi:10.1364/A0.50.004788.

 URL https://opg.optica.org/ao/abstract.cfm?URI=ao-50-24-4788

- [38] F. S. Ponciano-Ojeda, F. D. Logue, I. G. Hughes, Absorption spectroscopy and Stokes polarimetry in a 87Rb vapour in the Voigt geometry with a 1.5 T external magnetic field, Journal of Physics B: Atomic, Molecular and Optical Physics 54 (1) (2020) 015401. doi: 10.1088/1361-6455/abc7ff.
- [39] A. Nguyen Tuan, D. Le Van, S. Doan Hoai, B. Nguyen Huy, Manipulating multi-frequency light in a five-level cascade eit medium under doppler broadening, Optik 171 (2018) 721-727. doi:https://doi.org/10.1016/j.ijleo.2018.06.148.

 URL https://www.sciencedirect.com/science/article/pii/S0030402618309586